Research Article

Shuguang Li, Nermeen Abdullah, Umair Khan*, Aurang Zaib, Samia Elattar, and Anuar Ishak

Computational study of cross-flow in entropy-optimized nanofluids

https://doi.org/10.1515/ntrev-2024-0084
received January 31, 2024; accepted July 24, 2024

Abstract: Nanofluids (NFDs) are becoming better understood as a result of substantial boost in thermal efficiency advances and the rate of energy exchange employed in requisite fuel dynamics and automotive coolants. Owing to its usage, computational scrutinization examines the cross-flow of an NFD past an expanding/contracting sheet with the impact of suction. In addition, the entropy and irregular generation/absorption effects are induced to compute/estimate the magnificent point of NFD flow. The innovative components of this study are Brinkman number, nanoparticle volume fraction, dimensionless temperature difference, expanding/contracting factor, irregular heat source/sink, and suction parameters. The boundary layers undergo a stream-wise process through expanding and contracting sheets. Also, the study makes use of numerical simulations to scrutinize the aspects of heat transport and cross-flow of NFDs. The fundamental partial differential equations of the current model are converted to ordinary differential equations by using similarity variables, and then they are exercised *via* the bvp4c approach. Therefore, parametric research has been used to frame the effects of embedded flow variables on the drag force, heat transfer rate, and entropy generation profiles. Multiple solutions are provided for a certain range of shrinking parameters as well as the mass suction parameter. The results suggest that the shear stress enhances due to suction f_{wa} and nanoparticle volume fraction $\varphi_{\mathrm{TiO_2}}$, while the heat transfer accelerates due to $\varphi_{\mathrm{TiO_2}}$ and heat source ($A_b^*, B_b^* > 0$) and decelerates due to heat sink ($A_b^*, B_b^* < 0$). In addition, a favorable comparison with the literature that is already out there has been found, and it shows a great deal of similarities.

Keywords: entropy generation, cross-flow, irregular heat source/sink, stretching/shrinking sheet, nanofluid

*** Corresponding author: Umair Khan,** Department of Mathematical Sciences, Faculty of Science and Technology, Universiti Kebangsaan Malaysia, UKM, Bangi, 43600, Selangor, Malaysia; Department of Mathematics, Faculty of Science, Sakarya University, Serdivan/Sakarya, 54050, Turkey; Department of Computer Science and Mathematics, Lebanese American University, Byblos, Lebanon; Department of Mechanics and Mathematics, Western Caspian University, Baku, 1001, Azerbaijan, e-mail: umair.khan@lau.edu.lb, umairkhan@sakarya.edu.tr
Shuguang Li: School of Computer Science and Technology, Shandong Technology and Business University, Yantai 264005, China, e-mail: sgliytu@hotmail.com
Nermeen Abdullah: Department of Industrial & Systems Engineering, College of Engineering, Princess Nourah bint Abdulrahman University, P.O. Box 84428, Riyadh, 11671, Saudi Arabia, e-mail: NMAbdullah@pnu.edu.sa
Aurang Zaib: Department of Mathematical Sciences, Federal Urdu University of Arts, Science & Technology, Gulshan-e-Iqbal Karachi, 75300, Pakistan, e-mail: aurangzaib@fuuast.edu.pk
Samia Elattar: Department of Industrial & Systems Engineering, College of Engineering, Princess Nourah bint Abdulrahman University, P.O. Box 84428, Riyadh, 11671, Saudi Arabia, e-mail: SAElattar@pnu.edu.sa
Anuar Ishak: Department of Mathematical Sciences, Faculty of Science and Technology, Universiti Kebangsaan Malaysia, UKM, Bangi, 43600, Selangor, Malaysia, e-mail: anuar_mi@ukm.edu.my

Nomenclature

A_b^*	exponentially decaying space coefficients
B_b^*	temperature-dependent heat source/sink
Br_b	Brinkman number
c_p	specific heat at constant pressure (J kg^{-1} K^{-1})
C_f	skin friction
Nu_x	local Nusselt number
f_{wa}	suction parameter
G'	dimensionless velocity
H	dimensionless temperature
$A_b^*, B_b^* > 0$	heat source parameter
$A_b^*, B_b^* < 0$	heat sink parameter
Pr	Prandtl number
Re_x	local Reynolds number
T_a	temperature of the nanofluid (K)
T_{wa}	constant temperature (K)
T_∞	free stream temperature (K)
$u_{\mathrm{wa}}(x_a)$	variable velocity at the surface of the sheet (m s^{-1})
x_a, y_a	Cartesian coordinates (m)
$v_{\mathrm{wa}}(x_a)$	mass suction/injection or transpiration velocity at the surface of the sheet

u_a, v_a velocities in the $\bar{x}_{\bar{a}}$, and $\bar{y}_{\bar{a}}$ directions, respectively ($m\,s^{-1}$)

Greek symbols

ε_b positive constant
γ_b expanding/contracting factor
μ absolute viscosity (Pa s)
υ kinematic viscosity ($m^2\,s^{-1}$)
k thermal conductivity ($W\,mK^{-1}$)
ρ density ($kg\,m^{-3}$)
φ nanoparticle volume fraction
Ω_b dimensionless temperature difference
η pseudo-similarity variable

Acronyms

BCs boundary conditions
EG entropy generation
2D two-dimensional flow
Bvp4c boundary value problem of fourth-order
TiO_2 titania nanoparticles
NFD nanofluid
PDEs partial differential equations
ODEs ordinary differential equations
SBES stable branch solutions
USBES unstable branch solutions

Subscripts

nf nanofluid
f regular fluid
w wall boundary condition
∞ far-field condition

Superscript

' derivative w.r.t. η

1 Introduction

There are many nanoparticles and nanometer-sized molecules present in a nanofluid (NFD). Although the structure and content of nanomolecules depend on carbides, metals, and carbon nanotubes, tiny particles are dispersed (added) in fluids to improve their heat transfer properties. Most often, the components that make up an NFD are mixed with average-sized nanoscale particles. NFDs are frequently utilized to create nanotubes, nanofibers, nanowires, nanoparticles, nanosheets, nanorods, *etc.* The most effective and practical methods have been developed and put into practice for the modeling of NFD flow models, while the addition of specific materials of a particular kind has increased the thermal conductivity of various fluids. Several engineering procedures use nanoparticles in fluids to improve heat transfer. Equipment like heat exchangers in heavy machinery, automobiles, and industries is highly dependent on effective energy transfer. With these applications in mind, Choi and Eastman [1] developed NFDs to enhance the heat transfer capabilities of ordinary fluids. Eastman *et al.* [2] discovered a 40% increase in thermal conductivity when copper nanoparticles are added to ethylene glycol at a 0.3% volume concentration. Khan and Pop [3] have numerically addressed the issue of laminar fluid flow that develops when a flat surface is stretched in an NFD. It was discovered that the reduced heat transfer is a diminishing function of every single dimensionless number. The numerical solution of the boundary layer flow caused by a linearly extending sheet in an NFD was inspected by Makinde and Aziz [4]. They observed that the convective heating, thermophoresis, and Brownian motion all get more intense as the local temperature rises, which causes the thermal boundary layer to thicken. The thermal conductivity performance of carbon nanotubes in fluid flow over a stretching sheet was discovered by Haq *et al.* [5]. Sheikholeslami *et al.* [6] discovered the impacts of Lorentz forces on free convective flow in the presence of NFD with thermal radiation. A two-dimensional time-independent flow conveying an NFD toward a thin needle was deliberated by Soid *et al.* [7] where the existence of multiple solutions was reported. Bakar *et al.* [8] looked into the stability analysis of mass suction impacts through a shrinking/stretching cylinder considering the nanoparticles. Kamal *et al.* [9] investigated the flow of a nanomaterial through a stretchable/shrinkable sheet with a chemical reaction effect. A two-dimensional magneto mixed convection flow induced by a shrinking/stretching plate in an NFD was investigated by Jumana *et al.* [10]. Johan and Mansur [11] examined the features of dusty nanomaterial flow and thermal transport analysis past a stretchable sheet with a slip boundary. They used three types of nanoparticles, namely, copper, alumina, and titania. Shahzad *et al.* [12] inspected the impact of the slip effect on the flow and heat transfer induced by a copper NFD with different shape factors through a heated stretched sheet and found that the platelet shape factor particles have a greater rate of heat transfer compared to other shape factors. The significant impacts of viscosity dependent on the temperature through the slip flow with the assessment of bioconvection by involving a Maxwell NFD across a stretchy sheet were examined by Khan *et al.* [13]. Yasmin *et al.* [14] investigated the 3D unsteady flow of an NFD across a Riga plate with convective and slip conditions. They observed that the slip effect reduces the velocity, whereas the Biot number enhances the temperature of the NFD. The effect of activation energy on the 3D buoyancy flow of Sutterby fluid from an extended bidirectional surface with dissipation and thermophoresis effects was inspected by Yasmin *et al.* [15]. Yasmin *et al.* [16] scrutinized the blood flow by utilizing a Casson hybrid NFD across a heated surface in porous media. The temperature profile is accelerated by increasing values of the space-dependent heat source factor, constant heat source, and Eckert number. Hussain *et al.* [17] inspected the impact of chemically reactive and heat-absorbing effects on the dissipative flow of an NFD driven by a stretchable surface with a radiation effect. Their results indicate that the strengths of radiation, magnetic effect, and dissipation effects lead to enhancement of the temperature.

The problem of sheet stretching or shrinking in a viscous fluid has received a lot of attention since it has numerous applications in physics, engineering, and other scientific disciplines. It frequently occurs in practical issues that have attracted a lot of research attention because of their wide range of significance in fields like the production of glass fiber, glass blowing, metal extrusion, transportation, microfluidics, paper production, hot rolling, space, and acoustics (see Fisher [18]). The boundary layer flow over an ongoing solid kind surface flowing at uniform motion was initially studied by Sakiadis [19] in light of these applications. Numerous authors [20–22] have thought about different elements of this problem and found similarity solutions since the groundbreaking research conducted by Crane [23], who provided an exact solution for the 2D steady flow caused by a stretchable surface in a quiescent fluid. Instead of focusing on the scenario of a stretched sheet, researchers instead looked at the scenario of a shrinking sheet. According to Goldstein [24], this new kind of flow of shrinking sheet is fundamentally a backward flow. The steady flow across a shrinkable sheet was studied by Miklavčič and Wang [25]. They discovered that mass suction is necessary to continue the flow across a shrinkable sheet. Waini *et al.* [26] examined the dependency of time-varying flow along with thermal transport across a shrinking/stretching sheet incorporated with hybrid NFDs and provided multiple solutions.

The examination of cross-flow began following the early studies by Prandtl [27] and Blasius [28] that included the laminar flow over a flat surface caused by thin viscosity. It appears that Prandtl [29] is the first to present the results for uniform gradients in pressure flow across a finite yawed cylinder. Cooke and Hall [30] and Eichelbrenner [31] examined various theoretical and numerical techniques that have been developed for simulating a generalized boundary layer 3D flow. Weidman [32] examined the boundary layer *via* cross-flow generated by plate motions that are transverse. The work of Weidman was recently expanded by Roşca *et al.* [33] by taking into account rotational stagnation point flow that transports the hybrid NFD along a permeable shrinking or stretching surface. It was discovered that both stretching and shrinking surfaces can have multiple solutions to the fundamental similarity equations.

The phenomena of an irregular heat sink or source have applications in both engineering and medicine, including the cooling of metallic sheets, the design of thrust bearings, the recovery of unrefined oil, *etc.* In the presence of an irregular heat sink/source, Tawade *et al.* [34] addressed the motion of the MHD unsteady thin film and heat transfer past a stretchable sheet. It was determined that irregular heat parameters are crucial to the effectiveness of heat transfer. Thumma *et al.* [35] revealed that the stretching of a sheet caused the MHD convective motion of an NFD to have a changeable heat sink or source. To obtain the solution, a well-known Keller-Box numerical approach was utilized. Kumar *et al.* [36] looked at the movement of a hybrid ferrofluid film and heat transfer in the inclusion of radiation and an erratic heat source/sink (EHS/EHS). The rate of heat transfer is believed to be greater in hybrid ferrofluids than in ferrofluids. In addition, the velocity of the fluid and temperature tend to decline as the film thickness increases. Areekara *et al.* [37] investigated the impact of an irregular heat source/sink on the fluid flow of an NFD past a nonlinear stretching sheet. They observed that positive correlations exist between the radiative heat flux and the rate of heat transfer. Negative sensitivity to the rate of heat transfer is shown by the exponential heat source. Akram *et al.* [38] discussed the concepts of non-linear stretching and EHS/SHS to describe the heat transfer through the stretchable cylinder. It is discovered that the temperature distribution in the fluid region is being disrupted by the non-linear stretching rate and the source of heat.

The scrutiny of second law analysis (SLA) or entropy generation (EG) in fluid flow and heat transport is a prominent area of study. Energy losses resulting from diffusion, chemical reactions, friction between solid surfaces, and fluid viscosity all contribute to the production of entropy in thermodynamic systems. As a result, the formation of EG has drawn a lot of attention to applications, including heat exchangers, turbo machinery, and

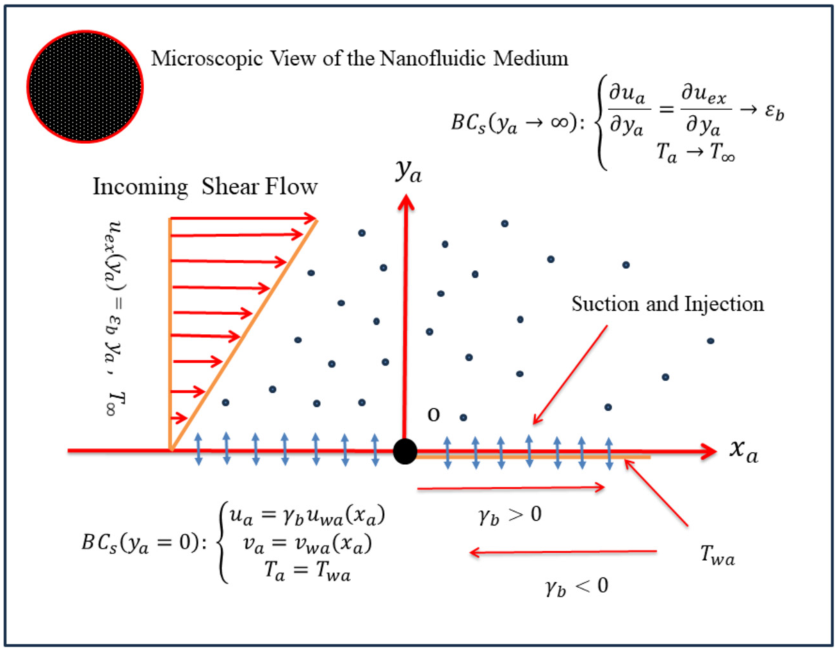

Figure 1: Physical model of the problem.

electronics cooling. Aiboud and Sauoli [39] scrutinized the entropy optimized in viscoelastic flow through a flexible surface subjected to the magnetic field. The effects of slip across a heated vertical surface in an entropy-optimized flow were calculated by Butt *et al.* [40]. Slips have been found to allow for the control and adjustment of entropy formation in thermal systems. Abolbashari *et al.* [41] employed HAM to examine EG in a magneto NFD flow near an unsteady stretched surface with a water-based fluid and several types of nanoparticles. Tlau and Ontela [42] examined the role of magnetohydrodynamics in a nanomaterial entropy-optimized flow through an inclined channel with a heat source/sink embedded in a porous media. Entropy optimization of nanomaterial flow across two stretchable rotating disks with effects of bioconvection was examined by Khan *et al.* [43]. Mondal *et al.* [44] used trapezoidal lid-driven enclosures with EG to study the Lorentz forces on the constant buoyant flow of Al_2O_3 nanoparticles. According to the calculations, the average Nusselt and Sherwood numbers and aspect ratios all decrease with increasing percentage of nanoparticle volume. Hussain [45] analyzed the EG on the unsteady magneto flow driven by non-Newtonian hybrid NFDs from a stretchable surface with a slip effect.

The literature that is currently accessible indicates that no studies have been conducted on the EG of the cross-flow induced by a nanomaterial past a stretching/shrinking sheet with significant impact on environmental and non-uniform heat generation/absorption. The present investigation fills a research gap by demonstrating cross-flow and heat transfer toward a stagnation point of NFD *via* a stretching/shrinking sheet with an irregular heat source/sink. Dual solutions are provided for certain values of parameters such as the mass suction and shrinking sheet. The proposed model is originally described *via* a highly nonlinear system of PDEs. The PDEs are converted into a set of ODEs by using appropriate similarity variables and then solved by employing a bvp4c solver.

The format of the article is as follows: Section 2 describes the description of the model. An SLA is developed in Section 3. Section 4 describes the numerical methodology, and Section 5 discusses the results of the problem. Finally, concluding remarks are provided in Section 6.

2 Description of the flow problem

The NFD stagnation point cross flow and thermal system characteristics past a stretching/shrinking surface with the mutual influence of mass suction and EHSE/EHSK are taken in this study. As portrayed in Figure 1, (x_a, y_a) are Cartesian coordinates measured along the horizontal and vertical surfaces of the sheet, respectively, with the flow occurring in the domain $y_a \geq 0$. An NFD is a mixture of regular fluid (water) and titania (TiO_2) nanoparticles. The investigational features of the (water/TiO_2) nanomaterials are assumed to be uniform. In addition, the horizontal surface of the sheet is assumed to have a variable velocity of

$u_a = \varepsilon_b^{2/3} v_f^{1/3} x_a^{1/3} \gamma_b = u_{wa}(x_a)\gamma_b$, where γ_b refers to the expanding/contracting factor with $\gamma_b < 0$, $\gamma_b > 0$, and $\gamma_b = 0$ signifying the particular cases of shrinking, stretching, and stationary/static sheets, respectively. ε_b indicates the positive constant and υ_f is the kinematic viscosity of the regular (water) fluid. The ambient or far-field (NFD) is also supposed to have a linear velocity of $u_{ex}(y_a) = \varepsilon_b y_a$, see Weidman [32]. Moreover, the mass suction/injection or transpiration velocity at the surface of the sheet is $v_{wa}(x_a)$, with $v_{wa}(x_a) < 0$ referring to the case of injection and $v_{wa}(x_a) > 0$ referring to the case of suction, while $v_{wa}(x_a) = 0$ indicating the impermeable surface of the sheet. It is also supposed that the constant temperature of the sheet is T_{wa}, while T_∞ represents the free stream temperature (inviscid fluid). With the help of these aforesaid assumptions, the governing equations in the Cartesian form are written as [32,33]:

$$\frac{\partial u_a}{\partial x_a} + \frac{\partial v_a}{\partial y_a} = 0, \tag{1}$$

$$\rho_{nf}\left(u_a \frac{\partial u_a}{\partial x_a} + v_a \frac{\partial u_a}{\partial y_a}\right) = \mu_{nf} \frac{\partial^2 u_a}{\partial y_a^2}, \tag{2}$$

$$\begin{aligned}(\rho c_p)_{nf}\left(u_a \frac{\partial T_a}{\partial x_a} + v_a \frac{\partial T_a}{\partial y_a}\right) &= k_{nf} \frac{\partial^2 T_a}{\partial y_a^2} + \frac{k_{nf} u_{wa}(x_a)}{x_a v_{nf}}[A_b^*(T_{wa} - T_\infty)e^{-\eta} \\ &\quad + B_b^*(T_a - T_\infty)],\end{aligned} \tag{3}$$

with the following boundary conditions (BCs):

$$\begin{aligned}&u_a = \gamma_b u_{wa}(x_a),\ v_a = v_{wa}(x_a),\ T_a = T_{wa} \quad \text{at} \quad y_a = 0, \\ &\frac{\partial u_a}{\partial y_a} \to \frac{\partial u_{ex}}{\partial y_a} = \varepsilon_b,\ T_a \to T_\infty \quad \text{as} \quad y_a \to \infty.\end{aligned} \tag{4}$$

In equations (1)–(4), u_a and v_a are the NFD velocities in the corresponding x_a and y_a directions, respectively; T_a refers to the temperature of the NFD; A_b^* refers to the exponentially decaying space coefficients; and B_b^* refers to the temperature-dependent heat source/sink. Therefore, the heat source or absorption phenomenon is produced due to the positive value of A_b^* and B_b^*, while the phenomenon of heat generation or sink is found by the negative value of both A_b^* and B_b^*.

Table 1: Physical aspects of (TiO_2/water) NFD

Physical properties	Water	TiO_2
ρ (kg/m^3)	997.1	4,250
c_p (J/kg K)	4179	686.2
k (W/mK)	0.613	8.9528
Pr	6.2	—

Furthermore, k_{nf} indicates the electrical conductivity (EC) of the essential posited NFD, $(\rho c_p)_{nf}$ indicates the heat capacitance of the NFD, ρ_{nf} indicates the density of the NFD, and μ_{nf} indicates the absolute viscosity of the NFD. The correlation of these NFDs is written as follows:

$$\begin{cases} k_{nf} = \dfrac{k_{TiO_2} + 2k_f - 2\varphi_{TiO_2}(k_f - k_{TiO_2})}{k_{TiO_2} + 2k_f + \varphi_{TiO_2}(k_f - k_{TiO_2})}, \\ \dfrac{(\rho c_p)_{nf}}{(\rho c_p)_f} = \varphi_{TiO_2}\left(\dfrac{(\rho c_p)_{TiO_2}}{(\rho c_p)_f}\right) + (1 - \varphi_{TiO_2}), \\ \dfrac{\rho_{nf}}{\rho_f} = \varphi_{TiO_2}\left(\dfrac{\rho_{TiO_2}}{\rho_f}\right) + (1 - \varphi_{TiO_2}),\ \dfrac{\mu_{nf}}{\mu_f} = (1 - \varphi_{TiO_2})^{-2.5}. \end{cases} \tag{5}$$

Here, k_f, ρ_f, and μ_f refer to the thermal conductivity, the density, and the absolute viscosity of the base (water) fluid, respectively, while the heat capacity at constant pressure is represented as c_p. Therefore, φ_{TiO_2} symbolizes the volume fraction of TiO_2 nanoparticles, and the special case $\varphi_{TiO_2} = 0$ reduces equation (5) to a normal or a regular fluid (water). In addition, Table 1 displays the physical data of TiO_2 nanoparticles and the regular fluid (water).

For the considered model, the similarity transformations that can be expressed to further simplify the procedure for mathematical analysis are as follows:

$$\begin{aligned}&\eta = (\varepsilon_b/\upsilon_f)^{1/3}\frac{y_a}{x_a^{1/3}}, \quad u_a = \varepsilon_b^{2/3}\upsilon_f^{1/3}x_a^{1/3}G'(\eta), \\ &H(\eta) = \frac{T_a - T_\infty}{T_{wa} - T_\infty}, \\ &v_a = -\frac{\varepsilon_b^{1/3}\upsilon_f^{2/3}}{3x_a^{1/3}}[2G(\eta) - \eta G'(\eta)],\end{aligned} \tag{6}$$

which provides the opportunity to describe flows extremely broadly, regardless of the system size. Also, the prime corresponds to the derivative with respect to η, H is the non-dimensional temperature distributions profile, G describes the non-dimensional quantities, and G' is the dimensionless velocity profile. However, the mass suction/injection velocity at the surface of the sheet is written as:

$$v_{wa}(x_a) = -\frac{2}{3}\left(\frac{\varepsilon_b \upsilon_f^2}{x_a}\right)^{\frac{1}{3}} f_{wa}. \tag{7}$$

In equation (7), f_{wa} is the constant mass suction/blowing constraint with $f_{wa} = 0$, $f_{wa} < 0$, and $f_{wa} > 0$ which describe the phenomena of impermeable, blowing, and suction, respectively.

With the help of similarity transformations (6), the continuity equation (1) of the governing model is satisfied, while the rest of equations (2) and (3) change to the resulting known ordinary (similarity) differential equations (ODEs) as:

$$\frac{\mu_{\rm nf}/\mu_{\rm f}}{\rho_{\rm nf}/\rho_{\rm f}}G''' + \frac{2}{3}GG'' - \frac{1}{3}G'^2 = 0, \tag{8}$$

$$\frac{k_{\rm nf}}{k_{\rm f}}H'' + \frac{2}{3}{\rm Pr}\frac{(\rho c_{\rm p})_{\rm nf}}{(\rho c_{\rm p})_{\rm f}}GH' + \frac{\left(\frac{k_{\rm nf}}{k_{\rm f}}\right)\left(\frac{\rho_{\rm nf}}{\rho_{\rm f}}\right)}{\left(\frac{\mu_{\rm nf}}{\mu_{\rm f}}\right)}(A_b^* e^{-\eta} + B_b^* H) = 0, \tag{9}$$

along with BCs:

$$\begin{aligned} &G(0) = f_{\rm wa}, \quad G'(0) = \gamma_b, \quad H(0) = 1 \quad \text{at} \quad \eta = 0, \\ &G''(\eta) \to 1, \quad H(\eta) \to 0 \quad \text{as} \quad \eta \to \infty. \end{aligned} \tag{10}$$

In addition, equation (8) for the case of $\varphi_{\rm TiO_2} = 0$ is the same as equation (6.1) in the study of Weidman [32] when $\alpha = 1$, but equation (9) with some special effects has been not taken in the same reference paper. Moreover, the dimensionless model comprised the following distinct parameters such as the suction/injection $f_{\rm wa}$, the expanding/contracting γ_b, and the Prandtl number ${\rm Pr} = \upsilon_{\rm f}/\alpha_{\rm f}$.

2.1 Gradients

Shear stress and heat transfer are the two vital physical aspects of the assumed model that are of practical significance to apply by scientists or engineers. They are defined as follows:

$$\begin{aligned} C_{\rm f} &= \frac{\mu_{\rm nf}}{\rho_{\rm f} u_{\rm wa}^2}\left(\frac{\partial u_a}{\partial y_a}\right)\Bigg|_{y_a=0}, \\ {\rm Nu}_x &= -\frac{x_a k_{\rm nf}}{k_{\rm f}(T_{\rm wa} - T_\infty)}\left(-k_{\rm nf}\left(\frac{\partial T_a}{\partial y_a}\right)\right)\Bigg|_{y_a=0}. \end{aligned} \tag{11}$$

By incorporating equation (6) into equation (11), the following dimensionless form yields

$$C_{\rm f}\,{\rm Re}_x^{1/2} = \frac{\mu_{\rm nf}}{\mu_{\rm f}}G''(0),\ {\rm Re}_x^{-1/2}{\rm Nu}_x = -\frac{k_{\rm nf}}{k_{\rm f}}H'(0). \tag{12}$$

Hence, ${\rm Re}_x = \frac{x_a u_{\rm wa}}{\upsilon_{\rm f}}$ refers to the local Reynolds number.

3 SLA

EG, also known as SLA, is a necessary instrument for measuring the energy loss and depreciation in the effectiveness of engineering and industrial systems, such as rate and transport operations. As a result, the systems expend less energy, making EG analysis and comprehension crucial. The scenario of EG is taken into account for viscous Newtonian liquids with the inclusion of nanoparticles.

$${\rm EG} = \frac{k_{\rm nf}}{T_\infty^2}\left(\frac{\partial T_a}{\partial y_a}\right)^2 + \frac{\mu_{\rm nf}}{T_\infty}\left(\frac{\partial u_a}{\partial y_a}\right)^2. \tag{13}$$

Two fundamental elements are principally responsible for the EG in the contemplated cross-flow of viscous Newtonian NFDs. The first term in the statement, which is on the right-hand side, denotes the ensuing local heat transfer, and the final term, the consequent fluid friction or viscous dissipation. The SLA is defined as follows in the dimensionless form:

$${\rm NG}^* = \frac{x_a^2 T_\infty^2}{k_{\rm f}(T_{\rm wa} - T_\infty)^2}{\rm EG}. \tag{14}$$

The following formulas are obtained by incorporating the similarity transformations from equation (6) into equation (13). Hence,

$${\rm NG}^* = \frac{k_{\rm nf}}{k_{\rm f}}{\rm Re}_x H'^2 + \frac{\mu_{\rm nf}}{\mu_{\rm f}}{\rm Re}_x\frac{Br_b}{\Omega_b}G''^2, \tag{15}$$

where Ω_b is the dimensionless temperature difference and Br_b is the Brinkman number. Consequently, they are represented mathematically as:

$$\Omega_b = \frac{(T_{\rm wa} - T_\infty)}{T_\infty}, \quad {\rm Br}_b = \frac{\mu_{\rm f} u_{\rm wa}^2}{k_{\rm f}(T_{\rm wa} - T_\infty)}. \tag{16}$$

4 Methodology

This section demonstrates the analysis of the assumed cross-flow and the suspension of NFD for heat transfer. The requisite model equations are expressed as highly nonlinear ODEs (8) and (9) along with BCs (10) using similarity variables (6). A built-in function named bvp4c included in the MATLAB software is used to work out these equations numerically. It ought to be noted that the scheme of the finite difference is the foundation for the bvp4c package, which is further highlighted by the three-stage Lobatto IIIA procedure. To instigate the bvp4c method, the transmuted ODEs are modified into a first-order system by launching new-fangled variables. By establishing this process, let

$$G = A_1, G' = A_2, G'' = A_3, H = A_4, H' = A_5. \tag{17}$$

Substituting equation (17) into (8) and (9) along with BCs (10), we obtain first-order ODEs as follows:

$$\frac{\rm d}{{\rm d}\eta}\begin{pmatrix} A_1 \\ A_2 \\ A_3 \\ A_4 \\ A_5 \end{pmatrix} = \begin{pmatrix} A_2 \\ A_3 \\ \frac{(\rho_{\rm nf}/\rho_{\rm f})}{(\mu_{\rm nf}/\mu_{\rm f})}\left[\frac{1}{3}A_2^2 - \frac{2}{3}A_1A_3\right] \\ A_5 \\ \frac{1}{\left(\frac{k_{\rm nf}}{k_{\rm f}}\right)}\left[-\frac{2}{3}{\rm Pr}\frac{(\rho c_{\rm p})_{\rm nf}}{(\rho c_{\rm p})_{\rm f}}A_4A_2 - \frac{(k_{\rm nf}/k_{\rm f})(\rho_{\rm nf}/\rho_{\rm f})}{(\mu_{\rm nf}/\mu_{\rm f})}(A_b^* e^{-\eta} \right. \\ \left. + B_b^* A_4)\right] \end{pmatrix}, \tag{18}$$

with BCs

$$A_1(0) = f_{\mathrm{wa}}, A_2(0) = \gamma_b, \; A_4(0) = 1, A_3(\infty) = 1, A_4(\infty) = 0. \quad (19)$$

The code desired initial estimations at the posited mesh point to solve equation (18) and the corresponding conditions (19). The polynomial used in the collective type yields a continuous result. A fourth-order precision set that is equally distributed over the spatial intervals where the function is integrated provides the result. The limitation at a distance ($\eta \to \infty$) is replaced by the value ($\eta = \eta_\infty = 8$) in many successful boundary layer theory applications, and the relative error tolerance is pre-defined as 10^{-6}. Additionally, the residual of the smooth output serves as the basis for both the mesh selection and error control. The initial mesh comprises four identical discredited points in the range $(0, \eta_\infty = 8)$, and the mesh selection is then automatically changed using the bvp4c package. The problem now has two possible solutions, which means that the bvp4c package needed two alternative guesses for the unstable and stable solutions. The early initial guess for the first solution is quite straightforward, while choosing a guess for the second solution is fairly challenging. Merkin [46] and Weidman *et al.* [47] claim that the first solution is physically stable and reliable, but the second solution is unstable and not physically dependable since the outcome only exists for a specific range of shrinking sheet.

4.1 Validation of the MATLAB bvp4c solver

This subsection of work specifies the rationality or validity, accuracy, and correctness of the considered MATLAB bvp4c solver for the special limiting case. To confirm this rationality, the friction factor outcomes for both branches (stable and unstable) are obtained owing to several values of the shrinking constraint with prior research work when f_{wa} and $\varphi_{\mathrm{TiO_2}}$ are equal to zero. Table 2 displays the results as well as a comparison to those of previous research work/literature. Thus, we can conclude that our results are trustworthy because our data closely align with those that have already been published.

Table 2: Numerical comparison of outcomes for friction factor owing to several values of the shrinking parameter when f_{wa} and $\varphi_{\mathrm{TiO_2}} = 0$

$\gamma_b < 0$	Waini *et al.* [48]		Present study	
	Stable	**Unstable**	**Stable**	**Unstable**
0.1	0.993440	−0.017703	0.993440	−0.017703
0.2	0.971925	−0.018388	0.971925	−0.018388
0.3	0.931424	−0.000045	0.931424	−0.000045
0.4	0.864452	0.044824	0.864452	0.044824
0.5	0.752585	0.134657	0.752585	0.134657

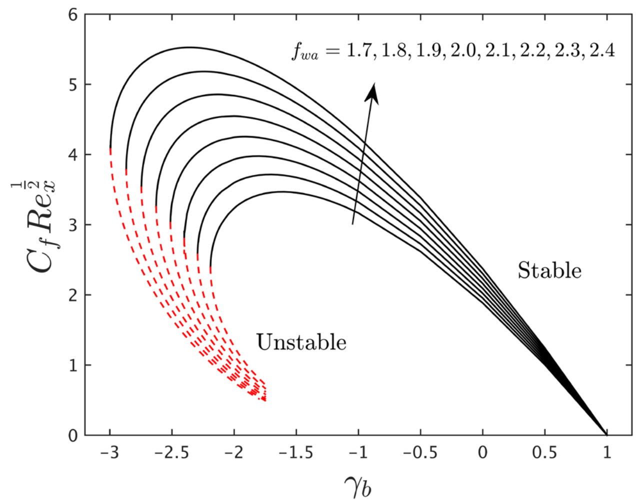

Figure 2: Impact of f_{wa} on $C_{\mathrm{f}}\,\mathrm{Re}_x^{1/2}$ *versus* γ_b.

5 Analysis of results

This section presents the binary (stable and unstable) solutions for a certain region or area of the dimensionless mass suction parameter as well as the contracting parameter γ_b due to the variations in one physical parameter at the time of computation while the other factors are assumed to be fixed. To ease analysis, the values of the basic physical influential parameters are set as $\varphi_{\mathrm{TiO_2}} = 0.025$, $\gamma_b = -2.0$, $f_{\mathrm{wa}} = 1.5$, $A_b^* = 0.1$, and $B_b^* = 0.1$. Table 1 reveals the

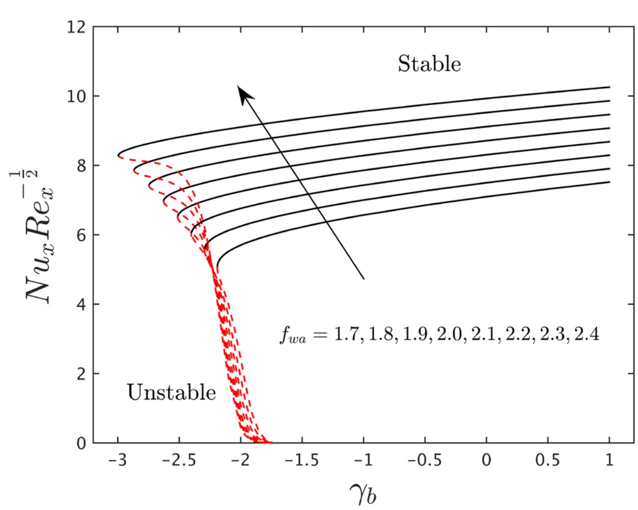

Figure 3: Impact of f_{wa} on $\mathrm{Nu}_x\,\mathrm{Re}_x^{1/2}$ *versus* γ_b.

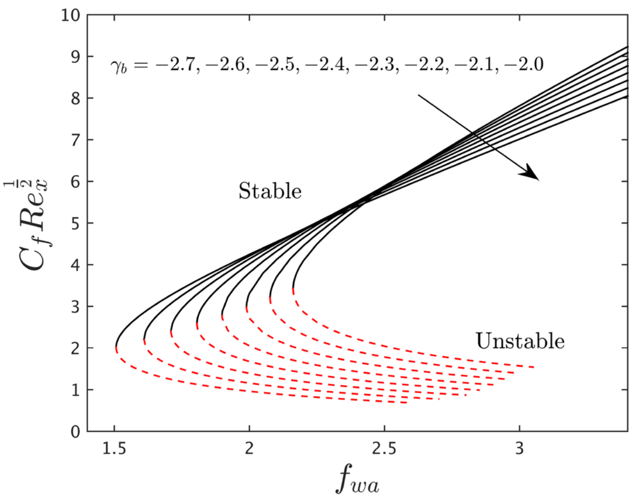

Figure 4: Impact of γ_b on $C_f\,\mathrm{Re}_x^{1/2}$ *versus* f_{wa}.

experimentation data of TiO_2 nanoparticles and the water-based liquid whose Prandtl number is 6.2. The comparison of the upshots for the unusual case is demonstrated in Table 2. The outcomes of the friction factor, heat transfer, and EG are captured in various graphs (Figures 2–8) of the NFD for the unstable and stable branches owing to the influence of several factors, and their quantitative outputs are shown in Tables 3 and 4. The branches of stable solutions (SBES) as well as those of unstable solutions (USBES) are indicated by the black solid and red dash lines, respectively, in the figures. The position in the graph or picture where both (SBES and USBES) curves meet at a single point is called the bifurcation or critical point. In this study, the SBES and USBES are invented only for the case of shrinking parameter.

The numerical data of gradients (friction factor and heat transfer) with the impression of several distinguished factors corresponding to water-based TiO_2 NFD are illustrated in Tables 3 and 4 for the SBSE and USBES, respectively. Upshots divulge that the friction factor upsurges for the SBSE owing to the superior values of φ_{TiO_2} and f_{wa}, while for the branch of USBES it behaves distinctly with variations in the mass suction parameter f_{wa} but similarly with higher impacts of φ_{TiO_2}. Notably, the shear stress of the NFD is the highest and lowest for the SBES and USBES with mass suction parameter f_{wa}. In contrast, the heat transfer escalates for both (SBES and USBES) results with superior consequences of φ_{TiO_2}. Therefore, owing to the rise in the heat source parameter $A_b^*, B_b^* > 0$, the heat transfer shrinkages in the SBES as well as the USBES, and it is endlessly enriching due to the higher role of the heat sink parameter $A_b^*, B_b^* < 0$. In addition, the lowest and highest heat

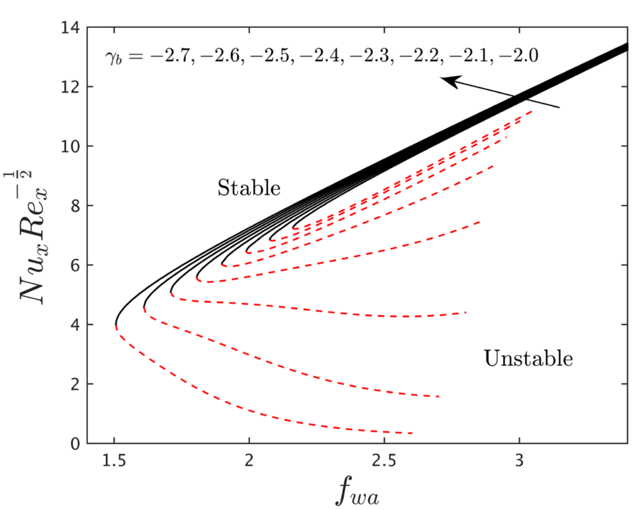

Figure 5: Impact of γ_b on $\mathrm{Nu}_x\,\mathrm{Re}_x^{1/2}$ *versus* f_{wa}.

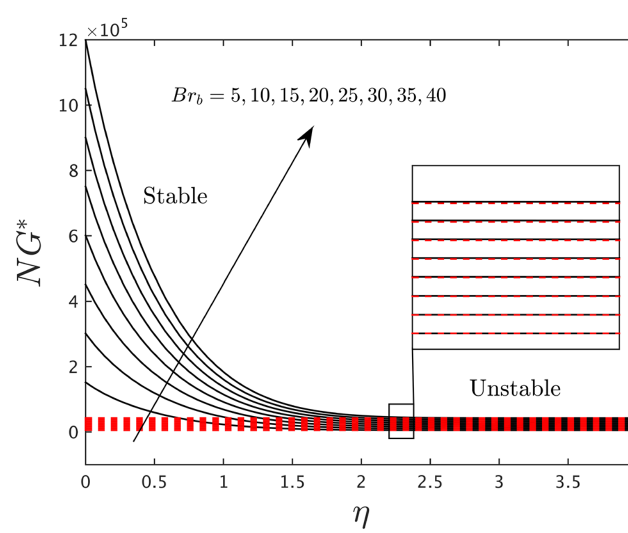

Figure 6: Impact of Br_b on NG^* *versus* η.

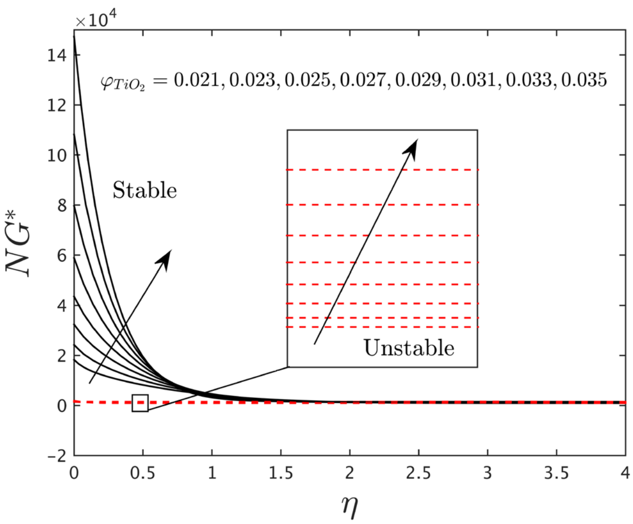

Figure 7: Impact of $\varphi_{\mathrm{TiO_2}}$ on NG* *versus* η.

Table 3: Numerical outcomes of shear stress with variations in $\varphi_{\mathrm{TiO_2}}$ and f_{wa}

$\varphi_{\mathrm{TiO_2}}$	f_{wa}	Shear stress	
		Stable	**Unstable**
0.025	1.5	5.6460767	1.0653406
0.030	—	5.8683445	1.0791223
0.035	—	6.0989946	1.0931549
0.025	1.5	5.6460767	1.0653406
0.030	2.0	8.1019827	0.7430102
0.035	2.5	10.531567	0.5628759

These dual (SBES and USBES) outcomes are based on specific parameters, including γ_b = 2.0, A_b^* = 0.1, and B_b^* = 0.1.

transfer approximations are perceived for the SBES and USBES with the following selected values A_b^*, B_b^* = 0.9 and $\varphi_{\mathrm{TiO_2}}$ = 0.035.

Figures 2 and 3 show the impact of f_{wa} on the shear stress and heat transfer corresponding to (TiO_2/water) NFDs for the SBES as well as the USBES, respectively. In this study, the dual (SBES and USBES) outcomes are possible to occur for a certain domain of specific set of physical parameters. Therefore, the non-unique outcomes in either pictures or graphs exist for a posited shrinkable sheet. Moreover, it is clear from the above graphs that the position where both solution curves meet is at a point called the critical point. Mathematically, this point is expressed by the symbol $\gamma_b C$, where the solutions are unique $\gamma_b = \gamma_b C$. The non-unique solutions (dual) and no solutions are possible to exist for the range $\gamma_b C < \gamma_b < \infty$ and $-\infty < \gamma_b < \gamma_b C$, respectively. Besides, the outcomes refer to the shear stress and heat transfer escalating for the SBES due to the larger impact of f_{wa}, while they are declined for the USBES. Physically, the motion of the NFD stops due to the inspiration of f_{wa} shifting the particles of the liquid moving toward the surface of the sheet and sticking with it. Hence, the friction and motion/velocity of the NFD hold the inverse relations; as a result, the shear stress is enhanced. Furthermore, the next eight distinct critical values −2.1903, −2.2941, −2.4016, −2.5125, −2.6274, −2.7463, −2.8686, and −2.9951 are obtained for the respective change value of f_{wa}. The rise of f_{wa} causes an increment in the absolute value of $|\gamma_b C|$. This behavior corresponds to the superior inclusion of f_{wa} decelerating the boundary layer separation.

The impact of γ_b on the shear stress and heat transfer *versus* f_{wa} of the (TiO_2/water) NFD for both (SBES and USBES) results are presented in Figures 4 and 5, respectively. The dual (SBES and USBES) results are shown in both graphs

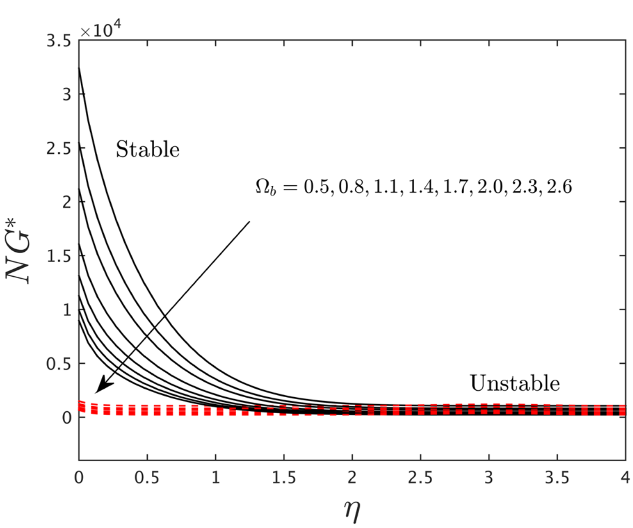

Figure 8: Impact of Ω_b on NG^* *versus* η.

Table 4: Numerical outcomes of heat transfer with variations in $\varphi_{\mathrm{TiO_2}}$ and A_b^*, B_b^*

$\varphi_{\mathrm{TiO_2}}$	A_b^*, B_b^*	Heat transfer	
		Stable	**Unstable**
0.025	0.5	4.6336867	15.001956
0.030	—	4.6360107	15.273743
0.035	—	4.6387796	15.562330
0.025	0.5	4.6336867	15.001956
—	0.7	4.3834284	10.021935
—	0.9	4.1226401	8.2234605
0.025	-0.5	5.7491768	4.6342404
—	-0.7	5.9488839	5.2367610
—	-0.9	6.1418652	5.6895740

These dual (SBES and USBES) outcomes are based on specific parameters, including γ_b = 2.0 and f_{wa} = 1.5.

for the case of f_{wa} due to the variations in the shrinking parameter. In both graphs, it is seen that the SBES and USBES curves meet at a point called the critical point, which is denoted as $f_{wa}C$. Meanwhile, the outcomes are unique for the case when $f_{wa} = f_{wa}C$, but the phenomena $f_{wa}C < f_{wa} < \infty$ and $-\infty < f_{wa} < f_{wa}C$ indicate the non-unique outcome and no solution, respectively. Besides, the shear stress decays and rises for the SBES due to the higher values of γ_b, while it shrinks for the USBES. Alternatively, with the increase of γ_b, the thermal transport phenomenon uplifts for the SBES and declines for the USBES. More significantly, it is understood from the diagrams that bifurcation values like 2.1615, 2.0760, 1.9888, 1.8986, 1.8057, 1.7096, 1.6098, and 1.5066 are found due to the several values of γ_b. Also, it is noted here that the magnitude of the critical values $|f_{wa}C|$ is weakened once the shrinking parameter is boosted. This further specifies that the growth in the impacts of γ_b hastens the boundary layer (BL) separations.

With the assistance or support of EG or SLA, the thermodynamic system performance of water-based TiO_2 nanoparticles can be improved. Figures 6–8 describe the effect of parameters Br_b, φ_{TiO_2}, and Ω_b on the SLA corresponding to the posited NFD for the SBES and USBES, respectively. As premeditated in Figures 6 and 7, an improvement in both parameters of Br_b and φ_{TiO_2} results in an improvement of SLA for the branch of stable as well as unstable solutions. The SLA is also more susceptible to changes in this parameter Br_b value at the place close to the wall surface of the sheet. As increases η, susceptibility rapidly decreases. Therefore, the physical data and prior research findings are compatible with this occurrence. Conversely, Figure 8 is designed to inspect the parameter Ω_b on SLA of the (TiO_2/water) NFD for both (SBES and USBES). In general, the lower temperature difference between the wall and its surroundings is generally caused by larger values of Ω_b, which reduces SLA or EG. The aforementioned discussion leads to the conclusion that by altering the related parameters, the system's SLA value can be decreased to increase the solar radiation utilization system's effectiveness.

6 Conclusions

The theoretical inspection on a cross flow- and heat transfer-incorporated water-based TiO_2 NFD through a permeable stretching/shrinking sheet with an irregular heat source/sink has been explored. EG was used to analyze the heat transfer process after the development of a requisite computational model. Combined impacts of pertaining governing parameters like suction, expanding/contracting parameter, irregular heat source/sink parameter, and volume fraction of the nanoparticles on shear stress and heat transfer have been analyzed. The important points are gathered as follows:

- The shear stress is enhanced due to f_{wa} and φ_{TiO_2}, while the heat transfer is accelerated due to φ_{TiO_2}.
- The domain of dual solutions is increased and boundary layer separation is delayed with higher impacts of f_{wa}; however, it is decreased with larger γ_b.
- The heat transfer accelerates due to the heat source $(A_b^*, B_b^* > 0)$ and decelerates due to the heat sink $(A_b^*, B_b^* < 0)$.
- EG increases in the presence of Brinkman number and nanoparticle volume fraction in both solutions, while it decreases due to the higher impacts of the difference in temperature parameter in both solutions.

7 Practical applications

NFDs are becoming better understood as a result of the substantial boost in thermal efficiency advances and the rate of energy exchange employed in requisite fuel dynamics and automotive coolants. In addition, the study of EG or irreversibility analysis is relevant and useful in various applications: it has a low freezing temperature, which is of assistance for preventing the fluid from freezing in regions with lower temperatures or during night-time when solar radiation is insufficient. In addition, the significant applications of NFDs by incorporating the impact of EG have been studied theoretically in this article, which is within the scope of nanotechnology reviews.

8 Future direction

The present work can be further inspected by considering the time-dependent flow with different aspects like thermal radiation, magnetic field, viscous dissipation, *etc.* Also, the mass transfer with chemical reaction is incorporated. Innovative combinations of hybrid NFDs and ferrofluids can be explored by solving current industrial difficulties and integrating a deep understanding of the physical atmosphere.

Acknowledgments: The authors acknowledge the funding by the Universiti Kebangsaan Malaysia project number "DIP-2023-005." In addition, Princess Nourah bint Abdulrahman University Researchers Supporting Project number (PNURSP2024R730), Princess Nourah bint Abdulrahman University, Riyadh, Saudi Arabia.

Funding information: This research was funded by the Universiti Kebangsaan Malaysia project number "DIP-2023-005." In addition, Princess Nourah bint Abdulrahman University Researchers Supporting Project number (PNURSP2024R730), Princess Nourah bint Abdulrahman University, Riyadh, Saudi Arabia.

Author contributions: U.K. and A.Z.: conceptualization, methodology, software, formal analysis, validation, writing – original draft. S.L.: writing – original draft, data curation, investigation, visualization, validation. A.I.: conceptualization, writing – review and editing, supervision, resources, writing – original draft. N.A. and S.E.: validation, writing – review and editing, software, writing – original draft. All authors have accepted responsibility for the entire content of this manuscript and approved its submission.

Conflict of interest: The authors state no conflict of interest.

Data availability statement: All data generated or analyzed during this study are included in this published article.

References

[1] Choi SU, Eastman JA. Enhancing thermal conductivity of fluids with nanoparticles (No. ANL/MSD/CP-84938; CONF-951135-29). IL (United States): Argonne National Lab; 1995.
[2] Eastman JA, Choi SUS, Li S, Yu W, Thompson LJ. Anomalously increased effective thermal conductivities of ethylene glycol-based nanofluids containing copper nanoparticles. Appl Phys Lett. 2001;78(6):718–20.
[3] Khan WA, Pop I. Boundary-layer flow of a nanofluid past a stretching sheet. Int J Heat Mass Transf. 2010;53(11–12):2477–83.
[4] Makinde OD, Aziz A. Boundary layer flow of a nanofluid past a stretching sheet with convective boundary condition. Int J Therm Sci. 2011;50(7):1326–32.
[5] Haq RU, Nadeem S, Khan ZH, Noor NFM. Convective heat transfer in MHD slip flow over a stretching surface in the presence of carbon nanotubes. Physica B: Condensed Matter. 2015;457:40–7.
[6] Sheikholeslami M, Hayat T, Alsaedi A. MHD free convection of Al_2O_3-water nanofluid considering thermal radiation: a numerical study. Int J Heat Mass Transf. 2016;96:513–24.
[7] Soid SK, Ishak A, Pop I. Boundary layer flow past a continuously moving thin needle in a nanofluid. Appl Therm Eng. 2017;114:58–4.
[8] Bakar NAA, Bachok N, Arifin NM. Stability analysis on the flow and heat transfer of nanofluid past a stretching/shrinking cylinder with suction effect. Res Phys. 2018;9:1335–44.
[9] Kamal F, Zaimi K, Ishak A, Pop I. Stability analysis of MHD stagnation-point flow towards a permeable stretching/shrinking sheet in a nanofluid with chemical reactions effect. Sains Malay. 2019;48(1):243–50.
[10] Jumana SA, Murtaza MG, Ferdows M, Makinde OD, Zaimi K. Dual solutions analysis of melting phenomenon with mixed convection in a nanofluid flow and heat transfer past a permeable stretching/shrinking sheet. J Nanofluids. 2020;9(4):313–20.
[11] Johan NA, Mansur S. Boundary layer flow of dusty nanofluid over stretching sheet with partial slip effects. J Advan Res Fluid Mech. Therm Sci. 2021;87(2):118–26.
[12] Shahzad A, Liaqat F, Ellahi Z, Sohail M, Ayub M, Ali MR. Thin film flow and heat transfer of Cu-nanofluids with slip and convective boundary condition over a stretching sheet. Sci Rep. 2022;12:14254.
[13] Khan SU, Usman, Al-Khaled K, Hussain SM, Ghaffari A, Khan MI, et al. Implication of Arrhenius activation energy and temperature-dependent viscosity on non-Newtonian nanomaterial bio-convective flow with partial slip. Arab J Sci Eng. 2022;47:7559–70.
[14] Yasmin H, Hejazi HA, Lone SA, Raizah Z, Saeed A. Time-independent three-dimensional flow of a water-based hybrid nanofluid past a Riga plate with slips and convective conditions: A homotopic solution. Nanotechnol Rev. 2023;12:20230183.
[15] Yasmin H, Zeeshan Z, Alshehry AS. A theoretical stability of mixed convection 3D Sutterby nanofluid flow due to bidirectional stretching surface. Sci Rep. 2023;13:22400.
[16] Yasmin H, Mahnashi AM, Hamali W, Lone SA, Raizah Z, Saeed A. A numerical analysis of the blood-based Casson hybrid nanofluid flow past a convectively heated surface embedded in a porous medium. Open Phys. 2024;22(1):20230193.
[17] Hussain SM, Mishra MR, Seth GS, Chamkha AJ. Dynamics of heat absorbing and radiative hydromagnetic nanofluids through a stretching surface with chemical reaction and viscous dissipation. Proc Inst Mech Eng, Part E: J Proc Mech Eng. 2024;238(1):101–11.
[18] Fisher EG. Extrusion of Plastics. New York, NY: Wiley; 1976.
[19] Sakiadis BC. Boundary-layer behaviour on continuous solid surfaces: I. Boundary layer equations for two-dimensional and axisymmetric flow. Am Inst Chem Eng J. 1961;7:26–8.
[20] Chen CK, Char MI. Heat transfer of a continuous, stretching surface with suction or blowing. J Math Anal Appl. 1988;135:568–80.
[21] Gorla RSR, Sidawi I. Free convection on a vertical stretching surface with suction and blowing. Appl Sci Res. 1994;52:247–57.
[22] Ishak A, Nazar R, Pop I. Boundary layer flow and heat transfer over an unsteady stretching vertical surface. Meccanica. 2009;44:369–75.
[23] Crane LJ. Flow past a stretching plate. Z Angew Math Phys. 1970;21:645–47.
[24] Goldstein S. On backward boundary layers and flow in converging passage. J Fluid Mech. 1965;21:33–5.
[25] Miklavčič M, Wang CY. Viscous flow due to a shrinking sheet. Q Appl Math. 2006;64:283–90.
[26] Waini I, Ishak A, Pop I. Unsteady flow and heat transfer past a stretching/shrinking sheet in a hybrid nanofluid. Int J Heat Mass Transf. 2019;136:288–97.
[27] Prandtl L. Über Flüssigkeitsbewegung bei sehr kleiner Reibung. Verh. III. Int Math Kongr Heidelberg 484–91, Teubner, Leipzig; 1946.
[28] Blasius H. Grenzschichten in Flüssigkeiten mit kleiner Reibung. Z Math Phys. 1908;56:1–37.
[29] Prandtl L. On boundary layers in three-dimensional flow. Rep Aero Res Coun Lond. 1946;9829.
[30] Cooke JC, Hall MG. Boundary layers in three-dimensional. Prog Aeron Sci. 1962;2:221–82.
[31] Eichelbrenner EA. Three-dimensional boudary layers. Ann Rev Fluid Mech. 5eds. M. Van Dyke, W. G. Vincinti and J. V. Wehausen, Annual Reviews Inc., Palo Alto; 1973.

[32] Weidman P. Further solutions for laminar boundary layers with cross flows driven by boundary motion. Acta Mech. 2017;228:1979–91.
[33] Roşca NC, Roşca AV, Jafarimoghaddam A, Pop I. Cross flow and heat transfer past a permeable stretching/shrinking sheet in a hybrid nanofluid. Int J Numer Meth Heat Fluid Flow. 2021;31:1295–19.
[34] Tawade J, Abel MS, Metri PG, Koti A. Thin film flow and heat transfer over an unsteady stretching sheet with thermal radiation, internal heating in the presence of external magnetic field. Int J Adv Appl Math Mech. 2016;3:29–40.
[35] Thumma T, Beg OA, Kadir A. Numerical study of heat source/sink effects on dissipative magnetic nanofluid from a non-linear inclined stretching/shrinking sheet. J Mol Liq. 2017;232:159–73.
[36] Kumar KA, Sandeep N, Sugunamma V, Animasaun IL. Effect of irregular heat source/sink on the radiative thin film flow of MHD hybrid ferrofluid. J Therm Anal Calorim. 2020;139:2145–53.
[37] Areekara S, Mackolil J, Mahanthesh B, Mathew A, Rana P. A study on nanoliquid flow with irregular heat source and realistic boundary conditions: A modified Buongiorno model for biomedical applications. Z Angew Math Mech. 2021;102(3):e202100167.
[38] Akram M, Jamshed W, Shankar Goud B, Pasha AA, Sajid T, Rahman MM, et al. Irregular heat source impact on Carreau nanofluid flowing via exponential expanding cylinder: A thermal case study. Case Studies. Therm Eng. 2022;36:102171.
[39] Aiboud S, Saouli S. Entropy analysis for viscoelastic magneto-hydrodynamic flow over a stretching surface. Int J Nonlinear Mech. 2010;45:482–9.
[40] Butt AS, Munawar S, Ali A, Mehmood A. Entropy generation in hydrodynamic slip flow over a vertical plate with convective boundary. J Mech Sci Technol. 2012;26:2977–84.
[41] Abolbashari MH, Freidoonimehr N, Nazari F, Rashidi MM. Entropy analysis foran unsteady MHD flow past a stretching permeable surface in nanofluid. Powder Technol. 2014;267:256–67.
[42] Tlau L, Ontela S. Entropy generation in MHD nanofluid flow with heat source/sink. SN. Appl Sci. 2019;1:1672.
[43] Khan NS, Shah Q, Bhaumik A, Kumam P, Thounthong P, Amiri I. Entropy generation in bioconvection nanofluid flow between two stretchable rotating disks. Sci Rep. 2020;10:4448.
[44] Mondal P, Mahapatra TR, Parveen R. Entropy generation in nanofluid flow due to double diffusive MHD mixed convection. Heliyon. 2021;7:e06143.
[45] Hussain SM. Irreversibility analysis of time-dependent magnetically driven flow of Sutterby hybrid nanofluid: a thermal mathematical model. Waves Random Complex Media. 2022;1–32. doi: 10.1080/17455030.2022.2089369
[46] Merkin JH. On dual solutions occurring in mixed convection in a porous medium. J Eng Math. 1986;20:171–79.
[47] Weidman PD, Kubitschek DG, Davis AMJ. The effect of transpiration on self-similar boundary layer flow over moving surfaces. Int J Eng Sci. 2006;44:730–7.
[48] Waini I, Ishak A, Pop I. Transpiration effects on hybrid nanofluid flow and heat transfer over astretching/shrinking sheet with uniform shear flow. Alex Eng J. 2020;59:91–9.